

Nanoscale

Accepted Manuscript



This is an *Accepted Manuscript*, which has been through the Royal Society of Chemistry peer review process and has been accepted for publication.

Accepted Manuscripts are published online shortly after acceptance, before technical editing, formatting and proof reading. Using this free service, authors can make their results available to the community, in citable form, before we publish the edited article. We will replace this *Accepted Manuscript* with the edited and formatted *Advance Article* as soon as it is available.

You can find more information about *Accepted Manuscripts* in the [Information for Authors](#).

Please note that technical editing may introduce minor changes to the text and/or graphics, which may alter content. The journal's standard [Terms & Conditions](#) and the [Ethical guidelines](#) still apply. In no event shall the Royal Society of Chemistry be held responsible for any errors or omissions in this *Accepted Manuscript* or any consequences arising from the use of any information it contains.

Study of lateral Schottky contacts in WSe₂ and MoS₂ field effect transistors using scanning photocurrent microscopy

Ya Yi[†], Changming Wu[†], Hongchao Liu[†], Jiali Zeng[‡], Hongtao He^{‡,*}, and Jiannong Wang^{†,*}

[†]*Department of Physics, The Hong Kong University of Science and Technology, Clear Water Bay, Hong Kong, China*

[‡]*Department of Physics, South University of Science and Technology of China, Shenzhen, Guangdong 518055, China*

* *Address correspondence to: heht@sustc.edu.cn, phjwang@ust.hk*

ABSTRACT

Schottky contacts, formed at metal/semiconductor interfaces, always have large impact on the performance of field-effect transistors (FETs). Here, we report the experimental studies of Schottky contacts in two-dimensional (2D) transition metal dichalcogenides (TMDCs) FET devices. We use scanning photocurrent microscopy (SPCM) to directly probe the spatial distribution of the in-plane lateral Schottky depletion regions at the metal/2D-TMDC interfaces. The laser incident position dependent and gate voltage tunable polarity and magnitude of short-circuit photocurrent reveal the existence of the in-plane Schottky depletion region laterally extending away from the metal contact edges along the channel. This lateral depletion region length is estimated to be around several microns and can be effectively tuned by the gate and drain-source biases. Our results solidify the importance of lateral Schottky depletion region in the photoresponse of 2D TMDCs optoelectronic devices.

KEYWORDS: transition metal dichalcogenides transistor, lateral Schottky barrier, scanning photocurrent microscopy, photoresponse.

Introduction

Two-dimensional (2D) crystals of transition metal dichalcogenides (TMDCs) have been studied extensively in recent years. In comparison with gapless graphene, TMDCs are semiconductors with the band gap energy corresponding to a wavelength ranging from visible to infrared. This makes TMDCs very promising for future nano-electronics and -optoelectronics applications. Besides, the strong spin-orbit coupling arising from the *d*-orbitals of the transition metal element and the breakdown of the inversion symmetry in the monolayer limit can lead to the spin splitting of the valence band. Therefore, 2D TMDCs are also ideal platforms for studying the valley spintronics. For a more complete picture on the current status one can refer to review articles in Ref. [1-7] and references therein. Field effect transistors (FETs) based on monolayer and few-layer TMDCs have been successfully fabricated with high on/off ratio up to 10^8 , much higher than that of graphene.⁸ Nevertheless, previous studies have shown that the metal contacts to TMDCs materials usually form Schottky barriers, which strongly limit the device performance, as well as the study of intrinsic spin and valley physics of TMDCs⁹⁻¹². Although various methods have been devoted to alleviate the influence of Schottky barriers¹³⁻¹⁹, more direct and systematic investigations of the Schottky contact itself to TMDCs are still needed. Especially in the 2D limit of TMDCs, the Schottky contact is expected to give rise to a depletion region extending laterally in-plane along the device channel, which is very different from the conventional Schottky contacts in bulk semiconductors.^{20,21} Scanning photocurrent microscopy (SPCM) has been shown as an effective method to investigate such lateral Schottky depletion regions in various devices based on carbon nanotubes,^{20,22,23} silicon nanowires,²⁴ 2D TMDCs,^{25,26} black phosphorus,²⁷ *etc.* The depletion region length up to several microns has been reported. Besides, the SPCM studies also reveal that the lateral Schottky depletion region related photoresponse effects may lead to some novel applications of 2D TMDCs^{21,28,29}.

In this work, we systematically study the Schottky contacts between the metal (Cr/Ti) and TMDCs thin films (WSe₂/MoS₂) using the SPCM method. Spatially resolved short-circuit photocurrent images clearly show that the Schottky depletion region extends a few microns laterally along the channel in our FET devices. By applying a gate voltage to tune the Fermi level of the thin films or a drain-source voltage to control the Schottky barrier height, we can effectively change the magnitude and direction of the built-in electric field in these lateral depletion regions, and in turn the magnitude and polarity of the observed photocurrent with local illumination of a laser. The photocurrent of our FET devices thus shows strong dependence on the gate bias, the drain-source bias, as well as the laser incident position. Our work not only directly probes the lateral Schottky depletion region, but also reveals the important role of it in mediating the photoresponse of 2D material optoelectronic devices.

Experimentals

Multilayer WSe₂ and MoS₂ thin films were prepared by scotch tape based mechanical exfoliation of bulk crystals and then transferred onto heavily doped silicon substrate with a 270 nm SiO₂ capping layer. A 1 min dry etching with SF₆/O₂ plasma was used to pattern the WSe₂ and MoS₂ flakes into long strips. Metal contacts were defined by electron beam lithography, followed by thermal evaporation of 5nm Cr/100nm Au on WSe₂ and electron beam evaporation of 5nm Ti/100nm Au on MoS₂, respectively. The electrical transport and SPCM measurements were carried out in ambient air at room temperature using an Agilent B2912A precision Source/Measure Unit and a 532 nm laser coupled with a microscopic setup. A 100X Mitutoyo long WD objective lens was utilized to focus the laser beam into ~ 1 μm -sized spot. A Burleigh XY stage coupled with a Newport Universal Motion controller (Model ESP300) was employed to scan the sample with a step size of 0.2 μm . We have

investigated 4 WSe₂ and 6 MoS₂ FET devices in this work and consistent results were obtained.

Results and Discussions

Fig. 1(a) shows the optical image of the WSe₂ FET device. The thickness of the WSe₂ flake measured by atomic force microscopy is 9 nm. A back gate with the 270 nm SiO₂ as the gate dielectric is utilized to tune the Fermi level or carrier density of the flake. Fig. 1(b) shows the gate bias, V_g , dependence of drain-source current, I_{ds} , under different drain-source bias, V_{ds} , conditions. One can see that applying a gate voltage can effectively change I_{ds} . Especially when $V_g < -60$ V, a rapid increase of I_{ds} is observed. Such a change in I_{ds} implies that the Fermi level has been tuned close to the valence band edge of WSe₂. On the other hand, if a large positive V_g is applied, the Fermi level will be tuned towards the conduction band edge, which gives rise to an increase in I_{ds} , as shown in Fig. 1(b). It is worth pointing out that the effective tuning of the Fermi level of WSe₂ by a gate voltage indicates that the Fermi level pinning does not occur in our WSe₂ FET device.

In conventional Schottky contact, the relevant depletion region has been known to extend into the bulk of a semiconductor and the side effect, *i.e.* the lateral expansion of the Schottky depletion region, is negligible when discussing the current-voltage characteristics of the contact. But in our work, the WSe₂ flake has a thickness of only 9 nm. The formation of a Schottky contact would lead to an extension of the depletion region in-plane in the lateral direction along the channel, instead of the conventional depth direction. In order to probe such a lateral depletion region in our device, the SPCM technique is employed, where the device channel is scanned point by point with a micron-sized laser spot ($\lambda = 532$ nm, spot size: ~ 1 μm , step: 0.2 μm , power: ~ 2 kW cm⁻²) and the photocurrent (I_{ph}) of the device at each point is recorded simultaneously. Fig. 2(a) shows the SPCM image of our FET device at $V_g = -100$

V under zero drain-source bias. A line cut of the SPCM image as indicated by a dashed line is also shown in Fig. 2 (a). The positive direction of the photocurrent is defined from the drain to source electrode, i.e. the y-direction in Fig. 2(a). In regions near the two electrodes, strong short-circuit photocurrent (I_{sc}) is measured, which is in sharp contrast to the middle region with much weaker or even negligible photocurrent. In a previous numerical modelling related to scanning photocurrent microscopy of Schottky contact in Si-nanowire, it has been shown that the profile of SPCM in a long channel device is determined by the minority carrier diffusion length.³⁰ This conclusion is based on the local injection of free electrons and holes. However, 2D TMDCs are known to have large exciton binding energy of about 0.37 and 0.96 eV for the monolayer WSe₂ and MoS₂, respectively^{31,32}, and about 60 and 80 meV for their bulk counterpart,^{33,34} which are all much larger than the thermal energy at room temperature (~26 meV). Therefore, different from the previous SPCM study of Si-nanowires³⁰, in the SPCM study of our 2D WSe₂ and MoS₂ flakes the photo-excitations generate excitons instead of free charge carriers. That is, under laser illumination, excitons are locally created and then diffuse to the depletion regions where they dissociate into free charge carriers, i.e. electrons and holes by built-in electric field. In the presence of the built-in electric field, these electrons and holes drift in opposite directions, thus forming the short-circuit photocurrent. It is the diffusion of excitons toward the depletion region and subsequent dissociation in the region that determines the spatial photocurrent profile of our FET devices. As a result, the length of the region with strong photoresponse corresponds to the lateral depletion region length plus exciton diffusion length.

From the SPCM image in Fig. 2(a) with $V_g = -100$ V, the strong photoresponse region length can be roughly estimated from image as 2.8 μm near the source electrode and 2.0 μm near the drain electrode, respectively. Previous ultrafast transient photoluminescence spectra study of 2D TMDCs has revealed that the exciton diffusion length in a 10 nm thick WSe₂ film

is about 380 nm.³⁵ Similar work on MoSe₂ also shows that the exciton diffusion length is 400 and 600 nm in the monolayer and bulk limits, respectively.³⁶ These indicate that the strong photoresponse region length measured is dominated by the depletion region length instead of the submicron exciton diffusion length. Assuming the exciton diffusion length in our WSe₂ FET device to be 400 nm, the source and drain depletion region length at $V_g = -100$ V can be estimated as 2.4 and 1.6 μm , respectively. Note that similar depletion region length at the order of microns has also been reported in a previous SPCM study of depleted carbon nanotube devices.²⁰

Furthermore, the photocurrent direction is opposite in the source and drain depletion region. This indicates that the built-in field of the source and drain depletion region is in the $-y$ and y directions, respectively, as indicated by red arrows in Fig. 2(a). From the SPCM image, the corresponding schematic band diagram of our FET device can be derived (see Fig. 2(c)). Since the 5 nm Cr layer is thick enough to form a continuous film, the metal contact to WSe₂ is Cr instead of the mixture of Cr and Au.³⁷ As shown in Fig. 2(c), the Fermi level of WSe₂ at $V_g = -100$ V is close to the valence band edge (p-type). Since the work function of Cr is 4.5 eV³⁸ and the electron affinity of WSe₂ is 4.03 eV³⁹, the Fermi level of Cr should be above that of WSe₂ under flat band condition. When the WSe₂ flake is in contact with Cr, holes transfer from WSe₂ to Cr results in a downward bending of the energy bands of WSe₂ toward the WSe₂/Cr interfaces. Due to the 2D nature of the WSe₂ flake, a lateral expansion of the depletion region is thus expected near both the source and drain electrodes. The downward energy band bending indicates a built-in electric field in $-y$ and y directions in the source and drain depletion regions, respectively. With the laser incident in the source or drain depletion region, the corresponding built-in field will give rise to a negative or positive photocurrent, consistent with the experimental results shown in Fig. 2(a).

As the magnitude and direction of the built-in field is closely associated with the Fermi

level alignment in the FET device, one can change the built-in field by tuning the Fermi level of WSe₂ at different V_g . Fig. 2(b) shows the SPCM image and a line cut of the image measured under $V_g = 100$ V with zero drain-source bias condition. Indeed, the photocurrent in the source or drain depletion region reverses its direction when V_g is changed from -100 to 100 V. Similar to Fig. 2(c), the schematic band diagram is also derived for $V_g = 100$ V (see Fig. 2(d)). Since the Fermi level of WSe₂ at $V_g = 100$ V is close to the conduction band (n-type), instead of the valence band at $V_g = -100$ V, the Fermi level of WSe₂ is now above that of Cr under flat band condition, as shown in Fig. 2(d). This leads to an upward bending of the WSe₂ energy bands when the flake is in contact with Cr, which is contrary to the downward bending at $V_g = -100$ V shown in Fig. 2(c). As a result, both the built-in field and the resultant photocurrent in the source or drain depletion region reverses its direction when V_g changes from -100 V in Fig. 2(a) to 100 V in Fig. 2(b).

The results in Fig. 2 present the effective gate voltage tunability of the direction and magnitude of photocurrent in our FET device. In addition, the measured photocurrent also depends on the laser incident position, as Fig. 2(a) and 2(b) show that the photocurrent changes its direction when the laser position is scanned from the source to the drain depletion region, or vice versa. To further elaborate this laser incident position dependent photocurrent, Fig. 3 and inset show the measured I_{ds} - V_{ds} characteristics on another WSe₂ FET device at slightly n-type regime with $V_g = 100$ V but different laser incident positions. For comparison, the I_{ds} - V_{ds} curve measured in dark without laser illumination is also shown in Fig. 3. When the laser is incident in the source depletion region of the device, the I_{ds} - V_{ds} curve exhibits a rectifying behavior. A large photocurrent is only observed at positive V_{ds} with a value up to $1.5 \mu\text{A}$ at $V_{ds} = 1$ V, while the photocurrent at negative V_{ds} remains small with a value of -12 nA at $V_{ds} = -1$ V, which is about three orders of magnitude smaller than that at positive V_{ds} but still larger than that in dark (-4 nA at $V_{ds} = -1$ V). At positive V_{ds} , the source Schottky contact

is reverse biased. In this case, the external field direction is the same as that of the built-in field, which results in an increase of the electric field in the source depletion region. Therefore, when the laser is positioned in the source depletion region, laser excited excitons will be dissociated more efficiently, leading to a large photocurrent. On the contrary, at negative V_{ds} the source Schottky contact is forward biased, resulting in a decrease of the electric field in the source depletion region. The dissociation of excitons becomes inefficient, thus giving rise to a small photocurrent at negative V_{ds} . This rectifying phenomenon reveals the change of the built-in electric field strength in the source depletion region by V_{ds} . Similar rectifying I_{ds} - V_{ds} characteristic but with opposite polarity can also be observed when the laser is positioned in the drain depletion region, as shown in Fig. 3. With the laser incident in the drain depletion region, the measured photocurrent arises from the dissociation of excitons by the built-in field in the drain depletion region. At negative and positive V_{ds} , the drain Schottky contact is reverse and forward biased, respectively. Therefore, a large photocurrent is observed at negative V_{ds} , while a small photocurrent at positive V_{ds} . Since the depletion region only occurs in the vicinity of the source and drain electrode, no built-in field is expected in the middle of the device channel. As a result, no short-circuit photocurrent and rectifying I_{ds} - V_{ds} behavior is observed and the photocurrent is small with a value of 42 nA at $V_{ds} = 1$ V and -16 nA at $V_{ds} = -1$ V (see the inset of Fig. 3). This position dependent I_{ds} - V_{ds} characteristics were also observed in GaSe photo-detecting devices. The authors also ascribed the asymmetric current to the V_{ds} modulated effective electric field in the Schottky depletion regions.²⁹

To further investigate the modulation of the lateral depletion region length by V_{ds} more directly, we also performed the SPCM studies on another FET device fabricated with a MoS₂ flake of 2.8 nm thick, as shown in Fig. 4(a). The electrode is made of Ti/Au and the MoS₂ flake is n-type. Fig. 4(b)-(d) show the obtained SPCM image of the device at zero gate voltage with different V_{ds} . A line cut of each SPCM image along the dashed line is also shown

in Fig. 4 (b)-(d). With no V_{ds} applied, as shown in Fig. 4(b), the length of the lateral depletion region is estimated from SPCM image as $1.6 \mu\text{m}$ and $1.0 \mu\text{m}$ near the source and drain electrode, respectively. Here we assume the exciton diffusion length to be 400 nm . The corresponding built-in electric field directions which can be inferred from the photocurrent direction are indicated by red arrows in this Figure. When a positive V_{ds} ($= 10 \text{ mV}$) is applied, as shown in Fig. 4(c), the length of the source depletion region increases to $2.2 \mu\text{m}$, while that of the drain one decreases to $0.6 \mu\text{m}$. This is because the source and drain Schottky contact at a positive V_{ds} is reverse and forward biased, respectively. When a negative V_{ds} ($= -10 \text{ mV}$) is applied, as shown in Fig. 4(d), the source contact is forward biased and the drain one reverse biased. As a result, the length of the source depletion region decreases to $0.4 \mu\text{m}$ and that of the drain one increases to $1.6 \mu\text{m}$. These results clearly demonstrate the tunability of the lateral depletion region length by V_{ds} . Compared with the SPCM image in Fig. 4 (b) where $V_{ds} = 0 \text{ V}$, Fig. 4 (c) & (d) also show that stronger (or weaker) photoresponse is observed in reverse (or forward) biased Schottky depletion region, consistent with the rectifying I_{ds} - V_{ds} characteristic discussed in Fig. 3. Similar results were also observed in WS_2 and black phosphorus devices.^{25,26} However, our results are distinctly different from the study of few layer MoS_2 FET devices,⁴⁰ in which the photocurrent was greatly enhanced with a large and increasing V_{ds} . But, in that case, the laser was incident in the space-charge region induced by pinch-off in the FET channel, not in the Schottky depletion regions.

Based on the results in Fig. 4(b)-(d), we can also derive the corresponding schematic band diagrams as shown in Fig. 4 (e) and (f). Previous study has shown that the work function of Ti is 4.3 eV and the electron affinity of MoS_2 is around 4.0 eV .⁴¹ Therefore, an upward bending of the MoS_2 energy bands toward the MoS_2/Ti interfaces is expected in the n-type MoS_2 FET device, which is similar to the WSe_2 FET device at $V_g = 100 \text{ V}$ when the Fermi level is close to the conduction band. This upward bending gives rise to the built-in field in y

(or $-y$) direction and positive (or negative) photocurrent in the source (or drain) depletion region.

It should be noted that besides the photovoltaic effect, the photothermalelectric (PTE) effect could be another possible mechanism for the observed photoresponse in our devices.^{40, 42-43} Unlike the photovoltaic effect, the photocurrent generated by the PTE effect is mainly due to thermoelectric voltage in response to the temperature difference across the electrodes and TMDCs, and it quantitatively equals to the thermal voltage divided by the device resistance. Here, the thermal voltage is proportional to the local temperature increase in the junction as well as the difference in the Seebeck coefficients between electrodes and TMDCs. For zero gate bias, take our trilayer MoS₂ device for example, the temperature difference across the electrodes and the channel is simulated to be ~ 128 mK. The Seebeck coefficient of MoS₂ at zero gate voltage is calculated to be -3.4×10^2 $\mu\text{V}/\text{K}$ while the Seebeck coefficient of Ti/Au is negligible with respect to that of MoS₂.⁴² (See supplementary information for details) Hence, the thermalelectric voltage between the electrode and the channel is ~ -44 μV . At $V_g = 0$ V, our device resistance is larger than 5 M Ω , then the photothermalelectric current should not exceed 10 pA, which is at least 3 orders of magnitude smaller than the short-circuit photocurrent value we observed. Therefore, the PTE effect caused photocurrent can be safely ignored here.

The above results reveal the important role of lateral Schottky depletion region in the photoresponse of 2D WSe₂ and MoS₂ FET devices. The photocurrent can be significantly enhanced with laser incident in the source or drain depletion region instead of in the middle of the channel. Since the built-in field direction is opposite to each other in the source and drain depletion region, our results also indicate illuminating the device locally in the lateral source or drain depletion region would give rise to a larger photocurrent than global illumination. More importantly, one can apply gate bias V_g or drain-source bias V_{ds} to effectively change

the profile of lateral depletion region of the device. The direction and magnitude of the photocurrent can thus be tuned with V_g and V_{ds} , as well as the laser incident position. For the MoS₂ device under $V_{ds} = \pm 1$ V and zero gate bias conditions the photo-responsivity, which is defined as the photocurrent divided by the incident laser power, is about 250 mA/W with laser illuminated at source or drain regions ($V_{ds} = \pm 1$ V, $I_{ph} = \sim \pm 5$ μ A). These photo-responsivity values are about three orders of magnitude larger than 0.42 mA/W obtained under the same gate and drain bias but with global illumination in a previous study of exfoliated monolayer MoS₂.⁴⁴ Therefore, lateral Schottky depletion region is a very important factor one must take into account when designing optoelectronic device with 2D semiconductors.

Based on the length of the lateral depletion region obtained from the SPCM mapping of the MoS₂ device at $V_{ds} = 0$ V, we tried to estimate the carrier density by using the classical 3D Schottky barrier equation⁴⁵:

$$X_n = \left[\frac{2\epsilon_r\epsilon_0 V_s}{eN_d} \right]^{\frac{1}{2}} \quad (1)$$

where $\epsilon_r = 7.43$ is the relative dielectric constant for MoS₂, $\epsilon_0 = 8.85 \times 10^{-12}$ F/m, $e = 1.6 \times 10^{-19}$ C, and N_d is the charge carrier density. With the source depletion region length $X_n = 1.6$ μ m and assuming that the built-in potential barrier V_s to be 0.1 ~ 0.3 V,^{41, 46} the calculated N_d is about $3.3 \times 10^{13} \sim 9.7 \times 10^{13}$ /cm³. The calculated bulk carrier density can be converted to sheet carrier density n_s by multiplying the film thickness. The resultant n_s is about $9.2 \times 10^6 \sim 2.7 \times 10^7$ /cm². However, the carrier density in our MoS₂ FET device at zero gate voltage estimated by the output and transfer curves, is $\sim 9.3 \times 10^{10}$ /cm² (see supplementary information), which is much larger than that obtained with equation (1).⁴⁰ This suggests that the classical Schottky barrier equation for conventional bulk semiconductors cannot be directly applied to a 2D system and new theoretical models should be proposed to understand the 2D cases.

Conclusions

In conclusion, the SPCM studies of 2D TMDCs FET devices clearly demonstrate the existence of in-plane lateral depletion region of the Schottky contact. By applying a gate voltage and/or drain-source bias, we can effectively tune the profile of the lateral depletion region. The measured photocurrent strongly depends on the gate voltage and/or the drain-source voltage, as well as the laser incident position. Our results reveal the importance of lateral Schottky depletion region in the photoresponse of 2D semiconductor optoelectronic devices.

Conflict of Interest: The authors declare no competing financial interest.

Acknowledgment: A special thanks to Prof. Gerald Bastard and Prof. Steven Louie for helpful discussions and valuable suggestions. This work was supported in part by the Research Grants Council of the Hong Kong SAR under Grant Nos. 605213 and HKU9/CRF/13G-1, and in part by the National Natural Science Foundation of China under Grant Nos. 11204183 and 11374135. The electron-beam lithography facility is supported by the Raith-HKUST Nanotechnology Laboratory at MCPF (SEG HKUST08).

FIGURES

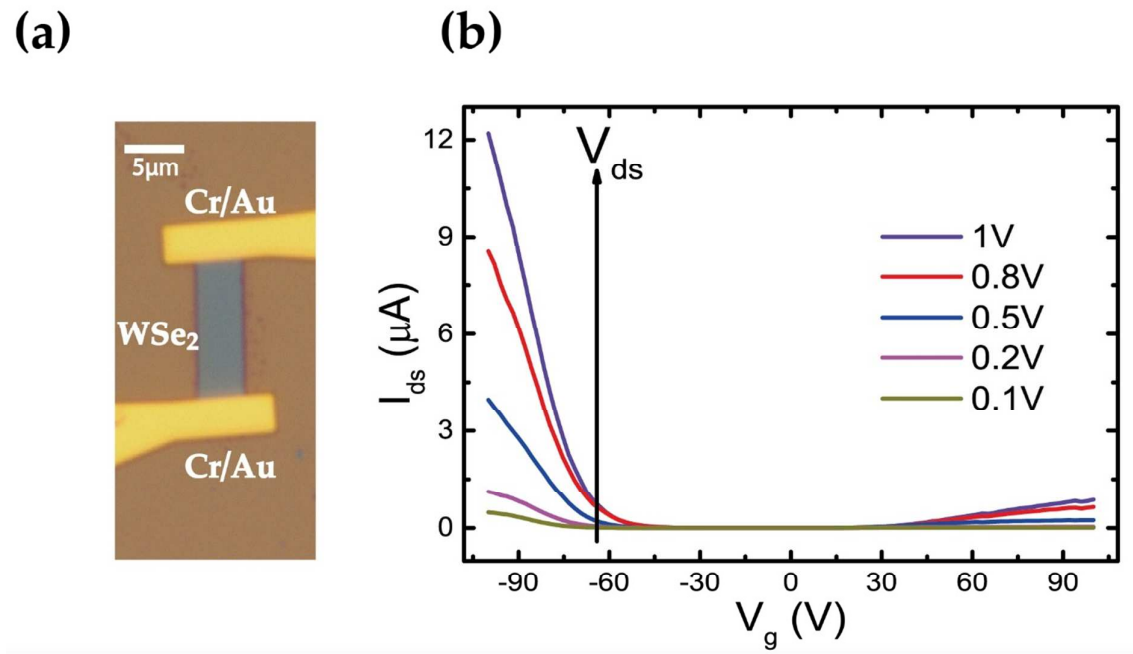


Fig. 1. (a) Optical image of mechanically exfoliated WSe₂ thin film contacted by Cr/Au electrodes. Scale bar: 5 μm . (b) Transfer curves for $V_{ds} = 0.1, 0.2, 0.5, 0.8, 1$ V of WSe₂ FET device.

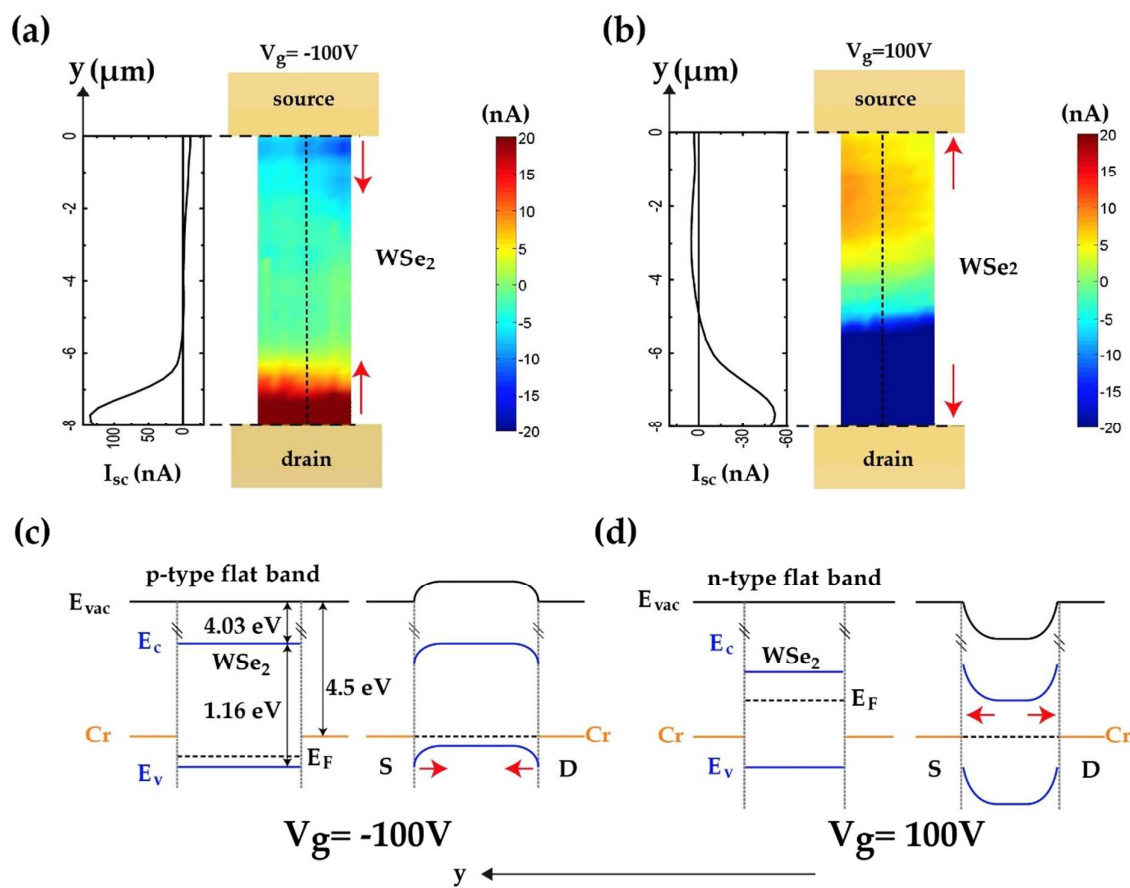


Fig. 2. Spatially resolved short-circuit photocurrent maps and corresponding line cuts at different transport regimes of a WSe₂ device, (a) $V_g = -100$ V, (b) $V_g = 100$ V. When $V_g = -100$ V, WSe₂ is in p-type regime while $V_g = 100$ V in n-type regime. Schematic band diagrams of WSe₂ device before (flat band) and after contacting with metal for (c) $V_g = -100$ V and (d) $V_g = 100$ V, respectively. The work function for Cr is ~ 4.5 eV.³⁸ The electron affinity and bandgap of WSe₂ are 4.03 eV and 1.16 eV, respectively.³⁹ The red arrows indicate the built-in electric field direction. The positive current direction is defined as flowing from D (drain) to S (source) in y direction.

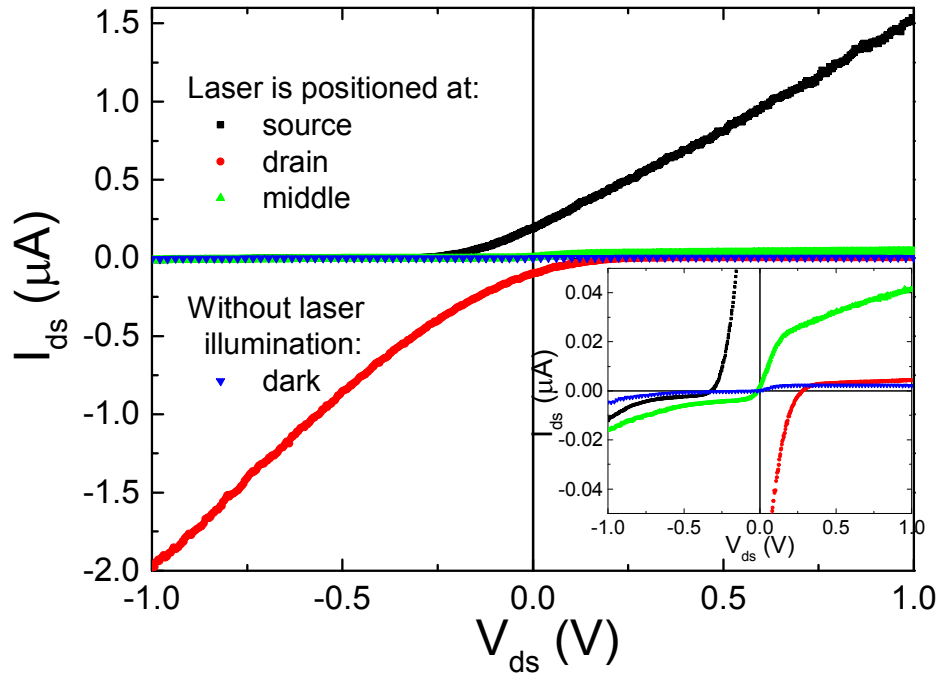


Fig. 3. I_{ds} - V_{ds} curves showing the photoresponse of WSe₂ FET device in n-type regime ($V_g = 100$ V). As indicated, the curves are measured with laser positioned at source, drain, and middle regions of the devices channel. The curve measured in dark without laser illumination is also shown. Inset: showing the portion of the curves with enlarged I_{ds} scale for clarity.

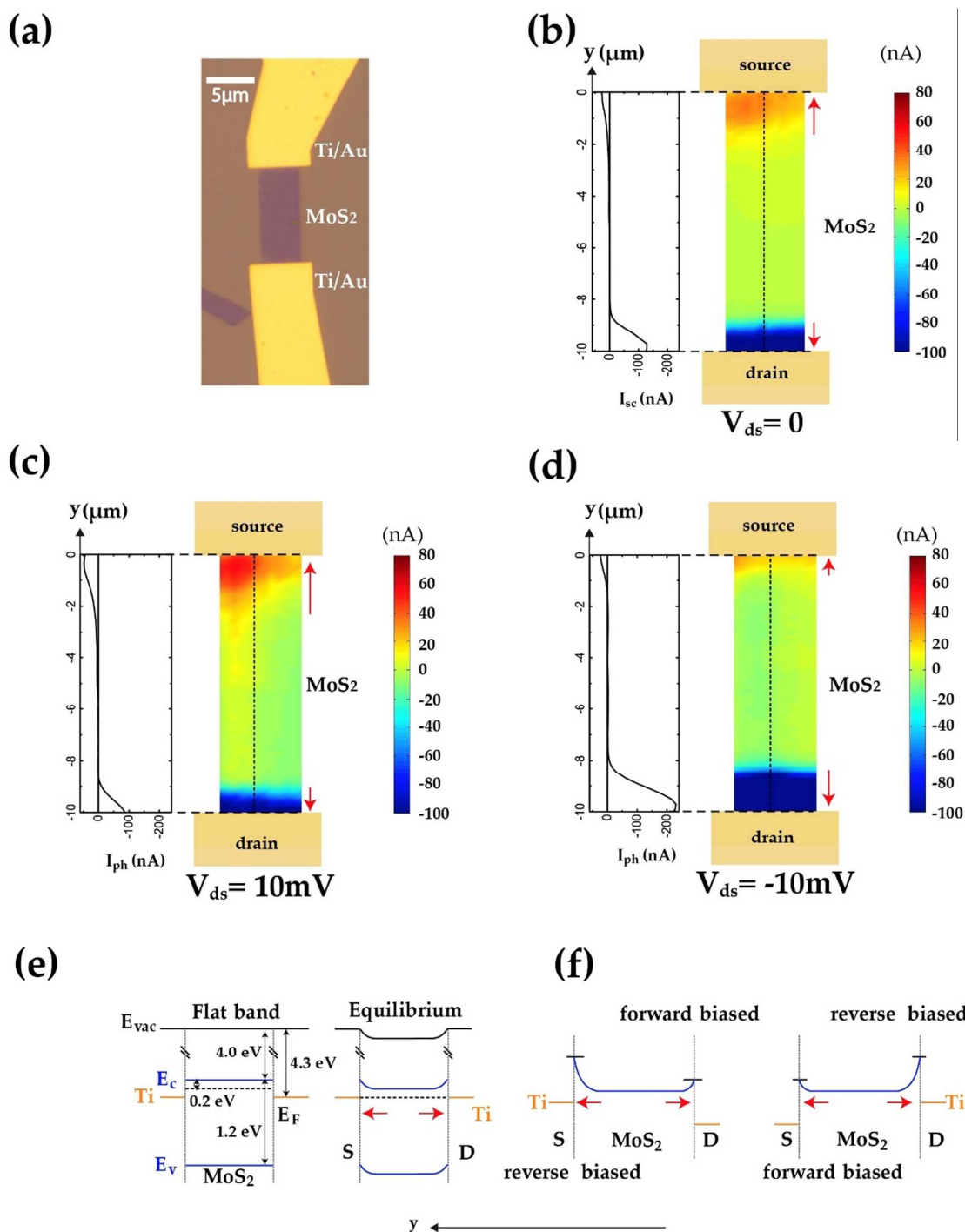


Fig. 4. (a) Optical image of MoS₂ thin film contacted by Ti/Au electrodes. Spatially resolved photocurrent maps with zero gate voltage and corresponding line cuts at $V_{ds} = 0$ V (b), 10 mV (c), and -10 mV (d), respectively. Schematic band diagrams of MoS₂ device before (flat band)⁴¹ and after contacting with metal for (e) $V_{ds} = 0$ V, (f) $V_{ds} = 10$ mV and -10 mV, respectively. The red arrows indicate the built-in electric field direction. The positive current direction is defined as flowing from D(drain) to S(source) in y direction.

References:

- 1 H. Xiao, Z. Zeng, H. Zhang. *Chem. Soc. Rev.*, 2013, **42**, 1934-1946.
- 2 H. Wang, F. Liu, W. Fu, Z. Fang, W. Zhou and Z. Liu, *Nanoscale*, 2014, **6**, 12250–12272.
- 3 F. Schwierz, R. Granzner and J. Pezoldt, *Nanoscale*, 2015.
- 4 Q. H. Wang, K. Kalantar-Zadeh, A. Kis, J. N. Coleman and M. S. Strano, *Nat. Nanotechnol.*, 2012, **7**, 699–712.
- 5 D. Jariwala, V. K. Sangwan, L. J. Lauhon, T. J. Marks, M. C. Hersam, *ACS nano*, 2014, **8**, 1102-1120.
- 6 X. Xu, W. Yao, D. Xiao, T. F. Heinz, *Nat. Phys.*, 2014, **10**, 343-350.
- 7 M. Buscema, J. O. Island, D. J. Groenendijk, S. I. Blanter, G. A. Steele, S. J. van der Zant, A. Castellanos-Gomez, *Chem. Soc. Rev.*, 2015, **44**, 3691.
- 8 B. Radisavljevic, A. Radenovic, J. Brivio, V. Giacometti and A. Kis, *Nat. Nanotechnol.*, 2011, **6**, 147–150.
- 9 H. Liu, M. Si, Y. Deng, A. T. Neal, Y. Du, S. Najmaei, P. M. Ajayan, J. Lou and P. D. Ye, *ACS nano*, 2013, **8**, 1031–1038.
- 10 N. Kaushik, A. Nipane, F. Basheer, S. Dubey, S. Grover, M. M. Deshmukh and S. Lodha, *Appl. Phys. Lett.*, 2014, **105**, 113505.
- 11 J. R. Chen, P. M. Odenthal, A. G. Swartz, G. C. Floyd, H. Wen, K. Y. Luo and R. K. Kawakami, *Nano. Lett.*, 2013, **13**, 3106–3110.
- 12 F. Ahmed, M.S.Choi, X. Liu, W. J. Yoo, *Nanoscale*, 2015, **7**, 9222.
- 13 W. Liu, J. Kang, D. Sarkar, Y. Khatami, D. Jena and K. Banerjee, *Nano. Lett.*, 2013, **13**, 1983–1990.
- 14 S. Das, H.-Y. Chen, A. V. Penumatcha and J. Appenzeller, *Nano. Lett.*, 2012, **13**, 100–105.
- 15 X. Liu, J. Hu, C. Yue, N. Della Fera, Y. Ling, Z. Mao and J. Wei, *ACS nano*, 2014, **8**,

- 10396–10402.
- 16 H. Fang, S. Chuang, T. C. Chang, K. Takei, T. Takahashi and A. Javey, *Nano. Lett.*, 2012, **12**, 3788–3792.
- 17 S. Chuang, C. Battaglia, A. Azcatl, S. McDonnell, J. S. Kang, X. Yin, M. Tosun, R. Kapadia, H. Fang, R. M. Wallace *et al.*, *Nano. Lett.*, 2014, **14**, 1337–1342.
- 18 Y. Liu, H. Wu, H. C. Cheng, S. Yang, E. Zhu, Q. He, M. Ding, D. Li, J. Guo, N. O. Weiss *et al.*, arXiv preprint arXiv:1412.7718, 2014.
- 19 C. Zhou, X. Wang, S. Raju, Z. Lin, D. Villaroman, B. Huang, W. Chan, M. Chan and Y. Chai, *Nanoscale*, 2015, **7**, 8695-8700.
- 20 M. Freitag, J. C. Tsang, A. Bol, D. Yuan, J. Liu and P. Avouris, *Nano Lett.*, 2007, **7**, 2037-2042.
- 21 W. Zhang, M.-H. Chiu, C.-H. Chen, W. Chen, L.-J. Li and A. T. S. Wee, *ACS Nano*, 2014, **8**, 8653–8661.
- 22 E. J. H. Lee, K. Balasubramanian, J. Dorfmuller, R. Vogelgesang, N. Fu, A. Mews, M. Burghard, K. Kern, K. *Small*, 2007, **3**, 2038 –2042
- 23 F. Léonard and J. Tersoff, *Phys. Rev. Lett.*, 1999, **83**,5174.
- 24 Y. Ahn, J. Dunning, J. Park, *Nano Lett.*, 2005, **5**, 1367–1370
- 25 H. Yamaguchi, J.-C. Blancon, R. Koppera, S. Lei, S. Najmaei, B. D. Magnum, G. Gupta, P. M. Ajayan, J. Lou, M. Chhowalla *et al.*, *ACS nano*, 2014, **9**, 840-849.
- 26 N. Ubrig, S. Jo, H. Berger, A. F. Morpurgo, A. B. Kuzmenko, *Appl. Phys. Lett.*, 2014, **104**, 171112
- 27 T. Hong, B. Chamlagain, W. Lin, H-J. Chuang, M. Pan, Z. Zhou, Y-Q. Xu, *Nanoscale*, 2014, **6**, 8978
- 28 S. Lei, F. Wen, B. Li, Q. Wang, Y. Huang, Y. Gong, Y. He, P. Dong, J. Bellah, A. George *et al.*, *Nano Lett.*, 2015, **15**, 259-265.

- 29 Y. Cao, K. Cai, P. Hu, L. Zhao, T. Yan, W. Luo, H. Zheng, *Sci. Rep.*, 2015, **5**, 8130.
- 30 D. Fu, J. Zou, K. Wang, R. Zhang, D. Yu, J. Wu, *Nano Lett.*, 2011, **11**, 3809-3815.
- 31 K. He, N. Kumar, L. Zhao, Z. Wang, K. F. Mak, H. Zhao, J. Shan, *Phys. Rev. Lett.*, 2014, **113**, 026803.
- 32 Y. D. Qiu, F. Jornada, S. G. Louie, *Phys. Rev. Lett.*, 2013, **111**, 216805.
- 33 A. Arora, M. Koperski, K. Nogajewski, J. Marcus, C. Faugeras, M. Potemski, *Nanoscale*, 2015, **7**, 10421-10429.
- 34 E. Fortin and F. Raga, *Phys. Rev. B.*, 1975, **11**, 905.
- 35 Q. Cui, F. Ceballos, N. Kumar, H. Zhao, *ACS nano*, 2014, **8**, 2970-2976.
- 36 N. Kumar, Q. Cui, F. Ceballos, D. He, Y. Wang, H. Zhao, *Nanoscale*, 2014, **6**, 4915-4919.
- 37 R. Birringer, C-H. Lu, M. Deal, Y. Nishi, R. H. Dauskardt, *J. Appl. Phys.*, 2010, **108**, 053704.
- 38 Weast. R.C, CRC Handbook of Chemistry and Physics, 2008, 12–114
- 39 S. McDonnell, A. Azcatl, R. Addou, C. Gong, C. Battaglia, S. Chuang, K. Cho, A. Javey, R.M. Wallace, *ACS nano*, 2014, **8**, 6265-6272.
- 40 C.-C. Wu, D. Jariwala, V. K. Sangwan, T. J. Marks, M. C. Hersam and L. J. Lauhon, *J. Phys. Chem. Lett.*, 2013, **4**, 2508–2513.
- 41 H. M.Li, D.Y. Lee, M. S. Choi, D. Qu, X. Liu, C. H. Ra, W. J. Yoo, *Sci. Rep.*, 2014, **4**, 4041.
- 42 M. Buscema, M. Barkelid, V. Zwiller, H. S. van der Zant, G. A. Steele and A. Castellanos-Gomez, *Nano Lett.*, 2013, **13**, 358–363.
- 43 Y. Zhang, H. Li, L. Wang, H. Wang, X. Xie, S-L. Zhang, R. Liu, Z. Qiu. *Sci. Rep.*, 2015, **5**, 7938.
- 44 Z. Yin, H. Li, H. Li, L. Jiang, Y. Shi, Y. Sun, G. Lu, Q. Zhang, X. Chen and H. Zhang,

ACS nano, 2011, **6**, 74–80.

45 D. A. Neamen and B. Pevzner, *Semiconductor physics and devices: basic principles*, McGraw-Hill New York, 2003, vol. 3.

46 M. Farmanbar and G. Brocks, arXiv preprint arXiv:1501.02130, 2015.